IEEE Access
Multidisciplinary | Rapid Review | Open Access Journal

Received February 13, 2019, accepted February 28, 2019, date of publication March 12, 2019, date of current version March 29, 2019.

Digital Object Identifier 10.1109/ACCESS.2019.2904647

High-Isolation Eight-Element MIMO Array for 5G Smartphone Applications

WEN JIANG, (Member, IEEE), BO LIU, YANGQIANG CUI, AND WEI HU, (Member, IEEE)
National Key Laboratory of Antennas and Microwave Technology, Xidian University, Xi'an 710071, China

Corresponding author: Wen Jiang (jw13@vip.qq.com)

This work was supported by the ZTE Industry-Academia-Research Cooperation Funds under Grant HC-CN-20171025026.

ABSTRACT In this paper, an eight-element MIMO array for 5G smartphone applications in the 3.45-GHz band (3.3–3.6 GHz) is presented. The array consists of two types of four-antenna arrays (U-shaped and L-shaped coupled-fed loop elements), which are symmetrically distributed in the inner of the smartphone frame. The dimension of the system circuit board is 124 mm × 74 mm and the size of two elements is 4.8 mm × 9.8 mm (0.055λ × 0.11λ, λ represents the free-space wavelength at 3.45 GHz) and 4.9 mm × 12.5 mm (0.056λ × 0.14λ), respectively. The proposed MIMO array is simulated, and a prototype is fabricated and tested. The results show that all the elements can cover the desired band of 3.3–3.6 GHz under the condition of −6-dB impendence bandwidth. The isolations are enhanced to 15 dB by combining the inverted-I ground slots with neutralization line (NL) structure. In addition, the envelope correlation coefficient (ECC) via any two elements is below 0.15 that shows good independence in far-field radiation characteristic. The measured efficiencies of the elements in the operating band are higher than 40%. Moreover, the array ergodic channel capacity is also calculated based on the correlation matrix method to be about 35 bps/Hz with a 20-dB signal-to-noise ratio. In addition, the effects of the user's hand and the head has been analyzed as well. Based on the above, the proposed eight-element MIMO array is a prospective candidate for future 5G smartphone applications.

INDEX TERMS Channel capacity, eight-element array, high isolation, MIMO antenna.

I. INTRODUCTION

In recent years, with the rapid development of wireless communication technology, the demands for high data rate and intelligent services are increasing [1], [2]. However, the explosive growth of data rate leads to a serious shortage of spectrum resources. It is known that MIMO technology can improve the channel capacity and the spectrum efficiency by exploiting multipath property without increasing the input power [3]–[5]. The more ports in MIMO system, the higher channel capacity can be obtained [6]–[11]. However, more antenna elements and closer distances between them will cause a more intense mutual coupling, thereby decreasing the performance of the MIMO system [12]. So, the key challenge to design MIMO array is to decrease the mutual coupling [13], [14]. Recently, some multi-element MIMO arrays include eight-, ten-, twelve- and even sixteen-antenna arrays have been presented in [9]–[11] and [15]–[17]. In [16], four compact two-antenna building block structures are utilized to constitute the eight-antenna MIMO array. The channel capacity is greatly improved by employing the eight elements, but the isolation is just 10dB. In addition, a sixteen-antenna array which elevated the channel capacity to 70bps/Hz has been studied [11]. The 10dB isolation is guaranteed by three neutralization lines. In [18], a 2×2 MIMO monopole array with a ground branch decoupling structure has been presented. It covers the band of 2.2-2.48GHz with high isolation (more than 20dB) and low ECC (less than 0.01). Meanwhile, a wideband dual-antenna has been studied [19], three neutralization lines are employed to ensure isolation, which is also adopted in [20]. Besides, orthogonally polarized technique has been used in [8], [9], [21], and [22]. In [21], a dual-polarized 4×4 MIMO antenna array composed of four orthogonal dipoles that are surrounded by thin copper has been demonstrated. The polarization diversity characteristic brings 20dB isolation to the array, as well as 11dB in [8]. Moreover, a 3×3 MIMO array by utilizing

The associate editor coordinating the review of this manuscript and approving it for publication was Haixia Cui.

TABLE 1. Performance comparison with previous published literatures.

Ref.	Decoupling Method	Total size	Spacing (edge to edge)	Isolation /dB	ECC	Channel capacity(with 20dB SNR)	Complexity
[10]	No	$140\times70\times0.8mm^3$ (ten-element)	17mm	10	<0.1	47bps/Hz (10×10)	
[26]	Defected ground	$25\times24\times1.6mm^3$ (two-element)	12.5mm	20	<0.04		Simple
[27]	Defected ground	$52\times77.5\times1.6mm^3$ (two-element)	15mm	>15	<0.5		Complex
[7]	Parasitic branches	$112\times100\times0.8mm^3$ (three-element)	27mm	20			Complex
[11]	Neutralization line	$150\times75\times0.8mm^3$ (eight- and sixteen-element)	>8mm	10	<0.32	34bps/Hz（8 ×8), 70bps/Hz (16×16)	Simple
[19]	Neutralization line	$115\times60\times0.8mm^3$ (two-element)	15mm	>15	<0.3		Medium
[8]	Polarization orthogonal	$136\times68\times0.8mm^3$ (eight-element)	>12.5mm	>12.5	<0.15	38bps/Hz	Simple
[9]	Polarization orthogonal	$150\times75\times6mm^3$ (twelve-element)	>6mm	>12.5	<0.2	57bps/Hz	Medium
[14]	Pattern diversity	$36\times36\times1.96mm^3$ (four-element)	>2mm	>10.8	<0.08		Simple
[28]	Pattern diversity	$160\times68.8\times0.8mm^3$ (eight-element)	>9mm	15	<0.15	36bps/Hz	Medium
This work	Hybrid decoupling (neutralization line and ground slot)	$124\times74\times6mm^3$ (eight-element)	17mm	>15	<0.15	35bps/Hz	Simple

the high-order modes decoupling has been presented [23]. The isolation is improved by placing the antenna elements in the stable null-amplitude field points. Furthermore, many other methods have been proposed to decrease the mutual coupling, such as ground slot structure [24], decoupling network [25], defected ground structure [26], [27], pattern diversity technique [14], [28], orthogonal-mode method [29], and the resonance structures [6], [30], [31]. In [25], a simple decoupling network based on a wide slot and a pair of narrow slots is employed to achieve good isolation between the dual-antenna groups. While, literature [26] presents a dual-band inverted-F MIMO antenna that the high isolation (about 15dB) is achieved by building two decoupling devices, a meandering resonant branch and an inverted T-shaped slot etched on the ground for the higher band and the lower band, respectively. Moreover, the pattern diversity technique is applied to change the electrical length of the radiators to manipulate the radiation pattern so that obtain a good isolation [14], [28]. In [29], the orthogonal-mode method is presented to mitigate the mutual coupling of the tightly arranged pairs. What else, some resonance structures, including the compact planar spiral line (PSL), the split-ring resonator structures (SRR) are also used to improve the isolation in [6], [30] and [31]. However, with the tendency of smart device miniaturization, there will be less and less space for antenna designing. Meanwhile, as for the MIMO antenna array, the isolations are close correlated with the bandwidth generally.

To solve the problem mentioned above, a high isolation printed eight-element array operating in the 3.45GHz band (3.3-3.6GHz) is investigated in this article. The array consists of two different four-antenna array which are placed on the side-edge of the frame symmetrically. In the proposed array, a good isolation is obtained by employing hybrid decoupling structures, including inverted-I ground slots and the grounded neutralization lines. The comparison between other decoupling designs and the proposed one is listed in table 1. Compared with other eight-element MIMO arrays, the proposed one has a smaller size and better isolation with hybrid decoupling structures.

II. ANTENNA ELEMENTS AND DECOUPLING STRUTURE

A. ANTENNA ELEMENTS

The geometries of two types of coupled-fed elements are displayed in Fig. 1. Both the U-shaped coupled-fed element (Ant1) and L-shaped coupled-fed element (Ant2) are designed to operate at 3.45GHz band. They are attached to the inner surface of the side-edge frame which is perpendicular to the ground plane. The size of the circuit board is 124mm×74mm and the height of the side-edge frame is only 6mm. The 0.8mm-thick FR4 substrate are used to

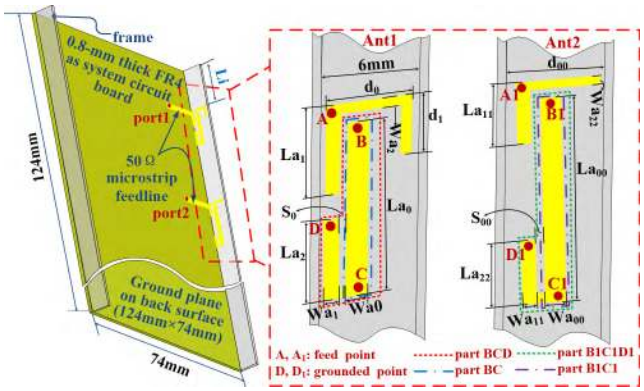

FIGURE 1. Geometries of two types coupled-fed loop antenna elements.

fabricate the frame and the circuit board, whose relative permittivity is 4.4 and loss tangent is 0.02.

The whole dimensions of the proposed two elements are 9.8mm×4.8mm and 12.5mm×4.9mm, respectively. Ant1 consists of a U-shaped coupled-fed strip, a radiated strip and a coupling aperture. Ant2 has the same structure as Ant1 except the feeding strip, which is shaped of L.

For Ant1, the U-shaped coupled-fed strip are marked with parameters of L_{a1}, W_{a1}, W_{a2}, d_0 and d_1. As the Fig.1 shown, the radiated strip (part BCD) surrounded by red dots line has dimensions of L_{a0}, W_{a0} and L_{a2}. Point D is grounded to the ground plane through a narrow strip. The coupling aperture between the feeding strip and part BC of the radiated strip has a width of S_0. The part BC is the main radiation portion at the front end of the radiated strip, which is marked out by blue dash dot line.

In addition, a 50Ω-microstrip line of width 1.5mm printed on upper surface of the substrate is used to feed at point A. The total length of Ant1 is 21mm (0.24λ, λ represents the free-space wavelength at 3.45GHz). It is known that the fundamental mode of traditional loop antenna is half-wavelength resonant mode, while the length of the proposed coupled-fed structure is just about quarter-wavelength. So, the size of antenna element is reduced effectively.

The feeding strip of Ant2 is shaped of L with parameters of L_{a11}, W_{a11}, W_{a22} and d_{00}. It is connected to the 50Ω-microstrip line at point A1. The radiated strip (part B1C1D1) surrounded by green dots line has dimensions of L_{a00}, W_{a00} and L_{a22}. Point D1 is grounded to the ground plane through a narrow strip. And the coupling aperture between the feeding strip and part B1C1 of the radiated strip has a width of S_{00}. The part B1C1 is the main radiation portion at the front end of the radiated strip, which is surrounded by purple dash dot line. The total length of Ant2 is 23.4 mm (about 0.26λ). The detail dimensions of the antenna parameters are listed in table 2. Fig. 2(a) shows the simulated reflection coefficients of the two elements in Fig. 1. And the effects of parameters d_{00} and d_1 are shown in Fig. 2(b). It can be seen that the bandwidth and the resonant frequency of antennas are related to d_{00} and d_1. The full-wave high-frequency

TABLE 2. Parameters of the antenna elements.

Parameters	L_{a0}	L_{a1}	L_{a2}	W_{a0}	W_{a1}	W_{a2}	S_0	d_0	d_1
Dimension (mm)	9.3	3	4.5	2.4	0.9	0.4	0.9	4.3	2.1
Parameters	L_{a00}	L_{a11}	L_{a22}	W_{a00}	W_{a11}	W_{a22}	S_{00}	d_{00}	
Dimension (mm)	10	5	4.5	1.6	0.8	0.7	0.8	3.7	

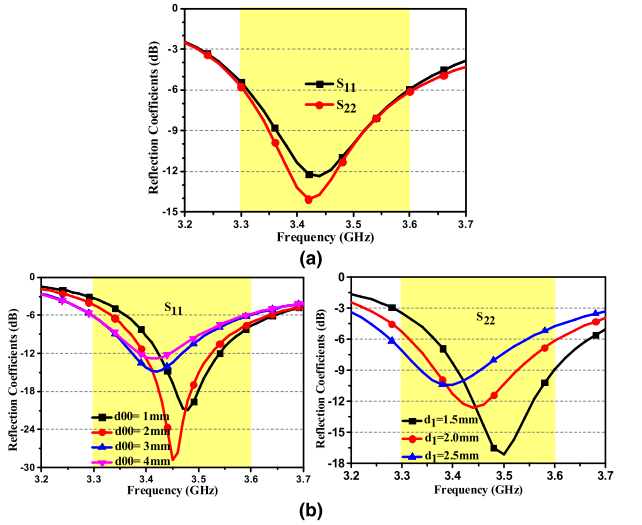

FIGURE 2. Simulated reflection coefficients of (a) U-shaped coupled-fed and L-shaped coupled-fed antennas, (b) effects of the parameters d_{00} and d_1.

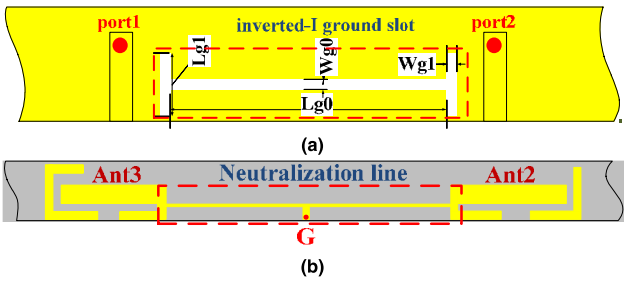

FIGURE 3. Geometry of decoupling structure (a) inverted-I ground slot, (b) neutralization line.

TABLE 3. Parameters of the inverted-I ground slot structure.

Parameters	L_{g0}	L_{g1}	W_{g0}	W_{g1}
Dimension(mm)	20	4.5	0.8	0.6

simulation software HFSS16 is applied for the simulation study.

B. DECOUPLING STRUCTURE

1) INVERTED-I GROUND SLOT

The geometric structure of inverted-I ground slots is shown in Fig. 3(a). It formed by three rectangular pieces including one horizontal and two vertical slots. All of them are etched at the edge of the ground plane. All the dimensions are displayed in table 3. The ground slot structure is equivalent to a filter, the

surface wave generated by the floor is constrained around the ground gap, reducing the effect of the excited port on the non-excited port. The slot resonance mode is determined by the total size of the slot structure that is related with the state at the edge of the slot. The isolation between antenna elements can be optimized efficaciously by adjusting the size and the position of the slot.

2) NEUTRALIZING LINE

The working mechanism of NL is that the induced current is neutralized by the conductive current transmitted on the NL, thereby reducing the mutual coupling. The proposed NL is a slender microstrip line with a width of 0.2mm, grounded at point G, as shown in Fig. 3(b). The NL is connected to the radiated strip of Ant2 and Ant3, and a good isolation can be obtained by adjusting the width of NL and the distance to ground.

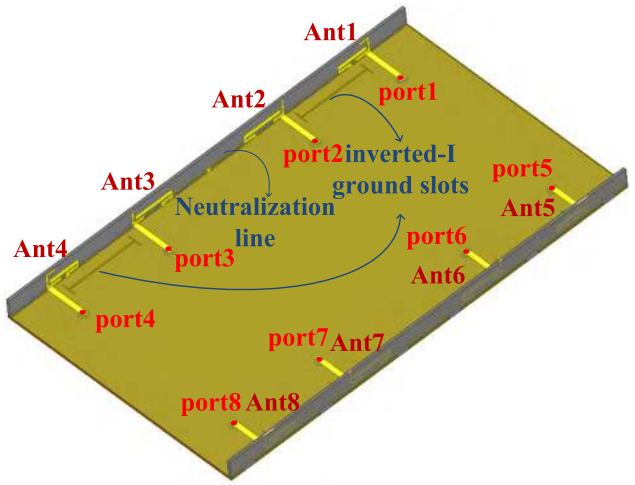

FIGURE 4. Configuration of the eight-antenna MIMO array.

III. EIGHT-ANTENNA MIMO ARRAY

A. ARRAY CONFIGURATION AND PERFORMANCES

Fig. 4 shows the configuration of the eight-element MIMO array (Ant1-Ant8), formed by two different four-antenna arrays. Array1 is composed of four U-shaped coupled-fed antennas, Ant1, Ant 4, Ant 5 and Ant8, which have the same size and are placed symmetrically on both sides of the frames. Array2 includes Ant2, Ant3, Ant6 and Ant7, which are L-shaped coupled-fed elements. They also have the same dimensions, and have the same arrangement as array1. As shown in Fig. 4, Ant1 and Ant2 are at a distance of 17 mm (0.2λ), so are Ant3 and Ant4. While, for Ant2 and Ant3, it is 22.4mm (0.26λ) apart. The distance from the unit Ant1 to the top of substrate is Li=6.4mm. For the MIMO array, with antenna numbers increases and the space decreases, the electromagnetic environment will become more complex, thereby the intense mutual coupling between antenna elements will be produced.

This design adopts two decoupling structures which are mentioned above, achieving a good isolation and impedance matching. Specifically, the inverted-I ground slot is etched upon the ground plane between Ant1 and Ant2, so does Ant3 and Ant4. The grounded neutralization line is utilized to connect radiated strips of Ant2 and Ant3.

For the Ant5-Ant8, they are similar with Ant1-Ant4. The 50Ω-SMA coaxial connectors are used to connect the ports of the eight-element array to the back of the system circuit board. The MIMO array shown in Fig. 4 has been fabricated and measured. The photo of the fabricated eight-element MIMO array is shown in Fig. 5.

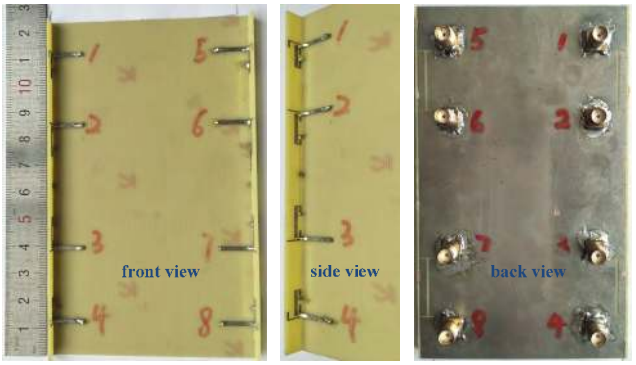

FIGURE 5. Photo of fabricated eight-antenna array.

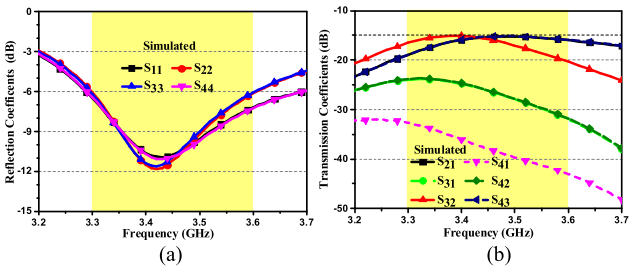

FIGURE 6. Simulated (a) reflection coefficients and (b) transmission coefficients of the eight-antenna array.

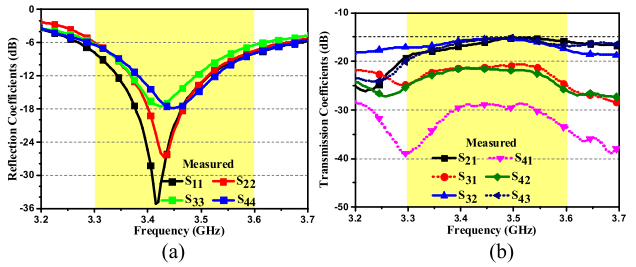

FIGURE 7. Measured (a) reflection coefficients and (b) transmission coefficients of the eight-antenna array.

The simulated and measured reflection coefficients and transmission coefficients of four representative antennas (Ant1, Ant2, Ant3 and Ant4) in the array are shown in Fig. 6 and Fig. 7, respectively. The performances of the Ant5-Ant8 is similar to Ant1-Ant4, because of the same structure and the same distribution.

The measured reflection coefficients and transmission coefficients of Ant1-Ant4 are revealed in Fig. 7, which

are in good accordance with the simulated ones in Fig. 6. The −6dB impedance bandwidth of the four antennas all cover the operating band (3.3-3.6GHz). The matching depth of S_{11}, S_{22} are better than S_{33}, S_{44}. The transmission coefficients S_{21}, S_{32} and S_{43} indicate a good isolation characteristic in the operating band. All of them are less than −15dB. In addition, the S31, S41 and S42 are smaller, less than −20dB.

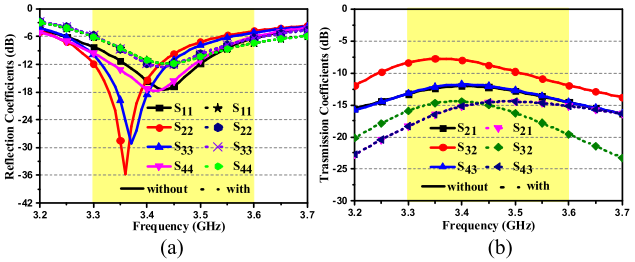

FIGURE 8. Simulated (a) reflection coefficients and (b) transmission coefficients of the eight-antenna array with or without the decoupling structure.

From Fig. 8(b), it can be known that the isolation is improved 4dB or more and the bandwidth is broadened by the decoupling structures.

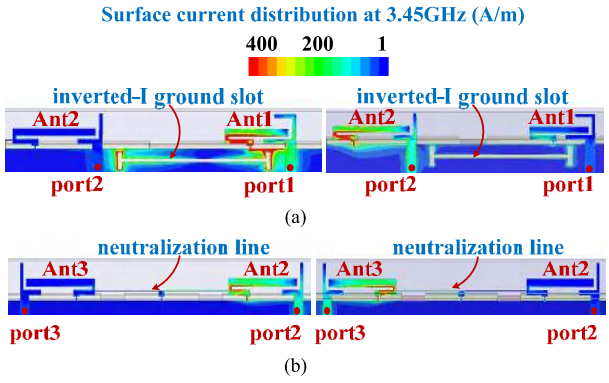

FIGURE 9. Simulated surface current distributions with decoupling structure (a) inverted-I ground slot, and (b) neutralization line.

Owing to the inverted-I ground slot structure, good isolation between Ant1 and Ant2 is obtained. The principle is shown in Fig. 9(a). When port1 is excited and port2 is terminated to 50Ω, the great majority of the excited surface currents on the ground plane is bounded around the slot, and it cannot enter port2. Similarly, when port2 is excited, the slot structure plays the same role. In addition, the induced current, generated by the mutual coupling, is neutralized by the conduction current on the neutralization line, which ensures the independence of Ant2 and Ant3. The surface current distributions are shown in Fig. 9(b).

The application of the hybrid decoupling structure is effective to decrease the surface wave coupling and inductive coupling. And it is worth mentioned that the isolations (better than 15dB) of proposed eight-element array are better than some eight-element MIMO arrays (just about 10dB) reported in [15] and [16]. Thus, the proposed hybrid decoupling method is very effective to 8×8 MIMO array decoupling.

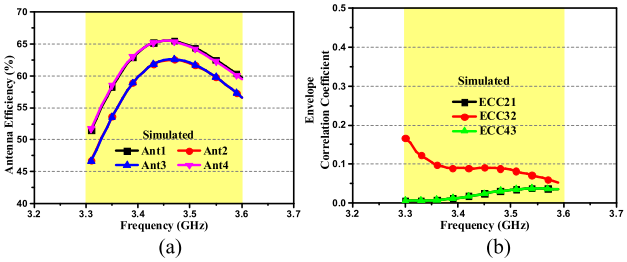

FIGURE 10. Simulated (a) antenna efficiencies and (b) ECC of the MIMO array.

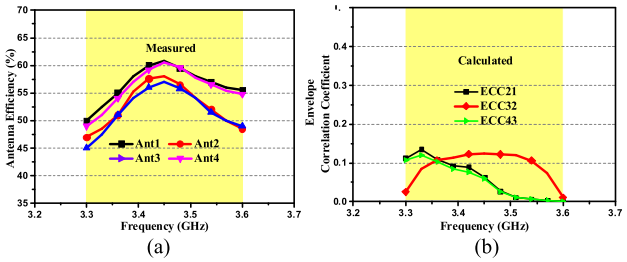

FIGURE 11. (a) Measured antenna efficiencies and (b) calculated ECC of the MIMO array.

Moreover, as shown in Fig. 11(a), the antenna efficiencies of Ant1-Ant4 measured in anechoic chamber are 45%-60% in the operating band, which are lower 2%–5% than the simulated ones in Fig. 10(a). That mainly caused by the mutual coupling, the loss of decoupling structure and test errors. Fig. 11(b) shows the calculated ECC based on the measured complex electric-field patterns of Ant1-Ant4, which are better than the simulation values in Fig. 10(b). The ECC is less than 0.15 for any two elements, which is good for MIMO applications.

All above analysis shows that the proposed decoupling scheme can improve the isolation of MIMO array under the premise of guaranteeing the bandwidth and small size.

In addition to the performances of the proposed MIMO array discussed above, the radiation pattern has also been analyzed. Because of the array structure mirror symmetry, the elements have the same radiation characteristics on symmetrical positions in theory. For brevity, only the one side elements are studied, including Ant1, Ant2, Ant3, and Ant4.

The simulated and measured radiation patterns in the yz-plane are shown in Fig. 12. It's obvious that the radiation patterns of Ant1 and Ant2 are different at the same plane and frequency due to the different structure.

As Fig. 12 shown that the measured results of the four elements are fluctuating to a certain extent around the simulated ones in some directions. This mainly due to the errors caused by the test environment and some external disturbances, but the overall trend of the two results are similar. It can be

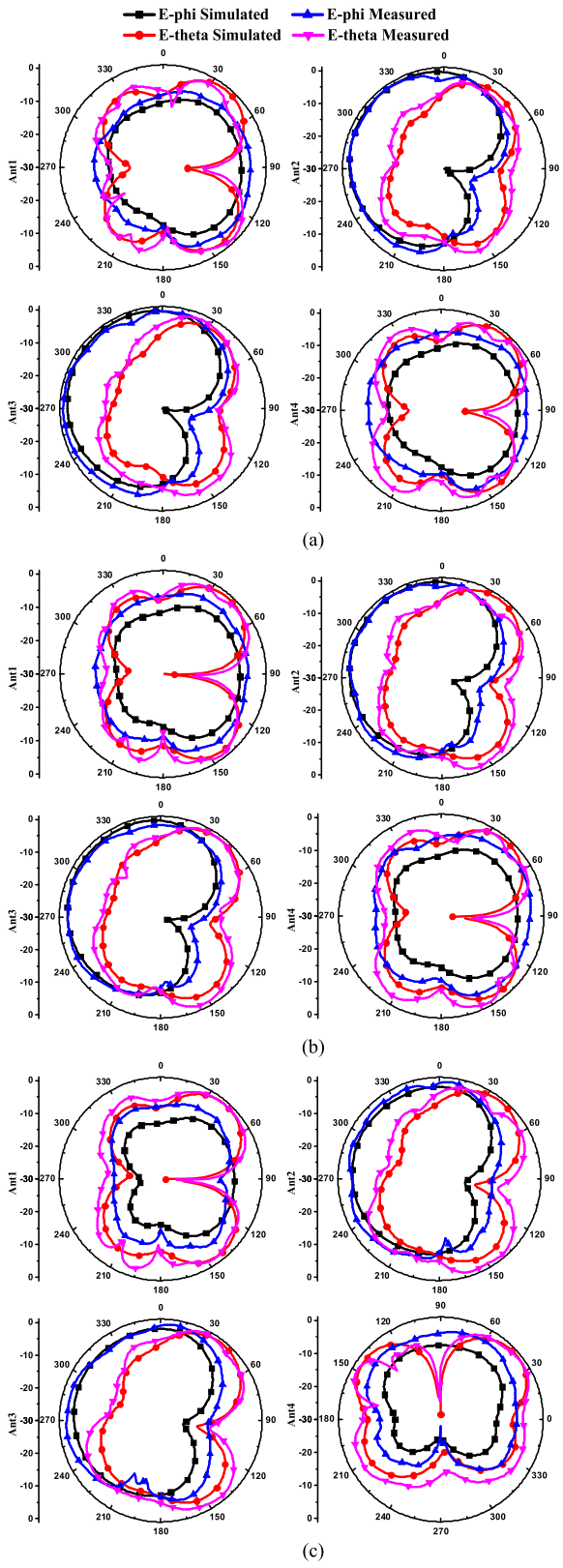

FIGURE 12. Simulated and measured radiation patterns of the Ant1, Ant2, Ant3, and Ant4 in the yz-plane of proposed U-shaped and L-shaped loop antenna elements at the different frequencies (a) 3.3GHz, (b) 3.45GHz, and (c) 3.6GHz.

seen from the E-phi component and its E-theta counterpart, the radiation pattern of the Ant1 and Ant4 are similar to that of a typical dipole antenna. The maximum radiating orientations of them are toward 45° and 135° directions, which near bi-directional patterns were observed in the yz-plane. While for Ant2 and Ant3, the maximum radiating orientations are toward 300° direction, differing from the Ant1 and Ant4.

Besides, as can be seen from Fig. 12(a), (b) and (c), the radiation pattern of the two types of elements remain unchanged at three frequency points, which indicates the pattern characteristics are relatively stable in the entire frequency band.

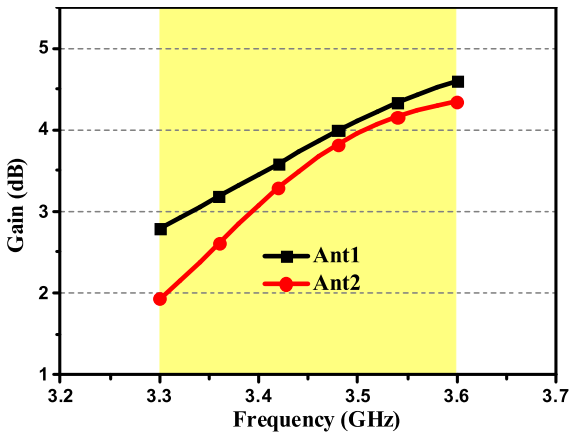

FIGURE 13. Gain of the two representative elements Ant1 and Ant2 in the operation band.

Fig. 13 shows the gain variation of the two representative elements Ant1 and Ant2 in the operation band, and the maximum gain of two elements are 4.8dB and 4.3dB, respectively.

B. THE CHANNEL CAPACITY OF THE MIMO ARRAY

The channel capacity of MIMO system is calculated by Shannon formula (1) usually. When calculating the channel capacity of the MIMO array, the channel model of the MIMO system should be selected at first, and the ray tracing model or the related statistical model are used generally. So, the channel capacity of the proposed 8×8 MIMO array mentioned above is calculated based on the correlation matrix method.

$$C = log_2 det(I + \eta \frac{SNR}{K} HH^H) \quad (1)$$

where I is an identity matrix, SNR denotes the mean SNR, K is the rank of the matrix HH^H, H is the channel matrix, and H^H denotes the Hermitian transpose of matrix.

As for the correlation matrix method, the key to calculating the channel capacity is to figure out the channel matrix [H] by the statistical method. As for the proposed MIMO array, the antennas are spaced by quarter wavelength under the non-line of sight condition in transmitter side and receiver side.

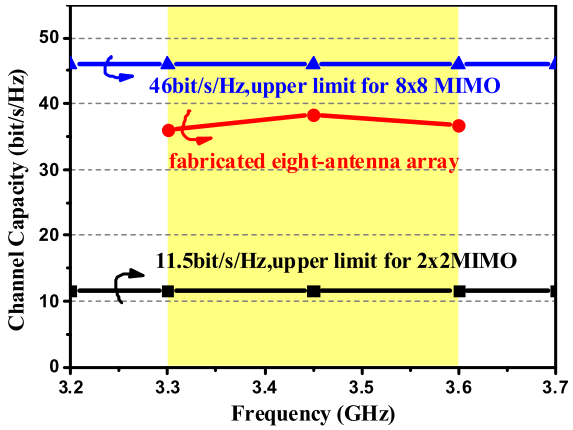

FIGURE 14. Calculated channel capacities of the eight-antenna MIMO array in an 8×8 MIMO system.

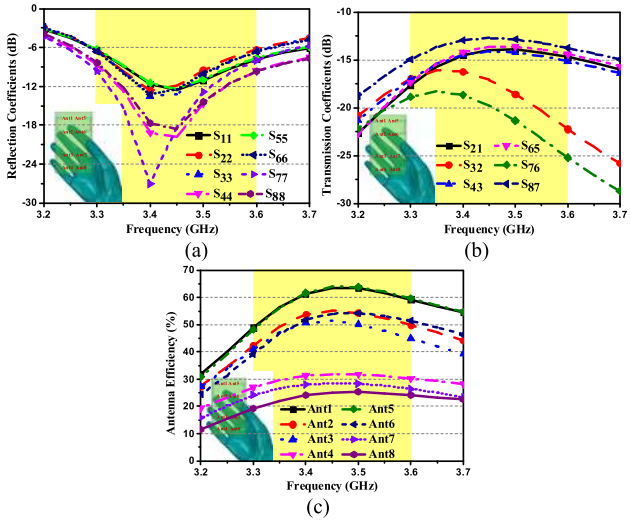

FIGURE 15. Simulated (a) reflection coefficients, (b) transmission coefficients and (c) antenna efficiencies of the MIMO array with single hand model.

The calculated channel capacity of the proposed array is indicated in Fig. 14, which is about 35 bps/Hz by considering measured efficiencies and averaging 80000 Rayleigh fading realizations with 20dB SNR in the identically and independently distributed propagation condition [12].

It is noted that the obtained channel capacity of the proposed 8×8 MIMO array studied here is about three times than a 2×2 MIMO system (upper limit 11.5 bps/Hz) with the same input power [32]. Compared the acceptable channel capacity here with that of an 8×8 MIMO system reported in [11], we can see that when a more extra 100MHz wide bandwidth in the 8×8 MIMO system, about the more 3 bps/Hz channel capacity can be improved.

C. USER'S HAND AND HEAD EFFECTS

For the design of terminal mobile antenna, it is indispensable to consider the effect of user's hand posture on the antenna performances. Three typical usage postures are considered in this paper, including single hand vertically holding handset, double hand horizontally holding mobile devices and the hand together with head's influence when answering the phone.

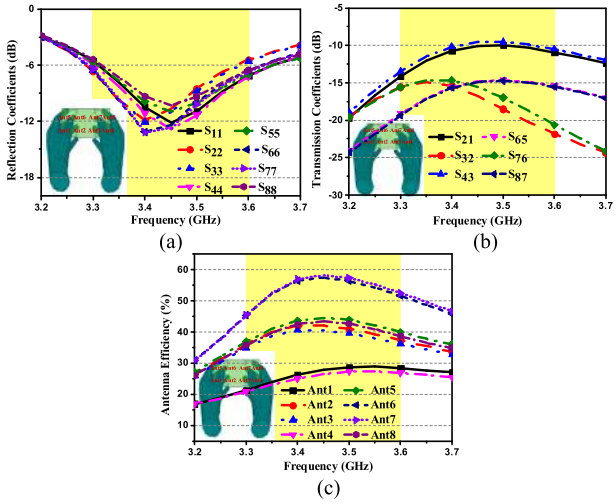

FIGURE 16. Simulated (a) reflection coefficients, (b) transmission coefficients and (c) antenna efficiencies of the MIMO array with double hand model.

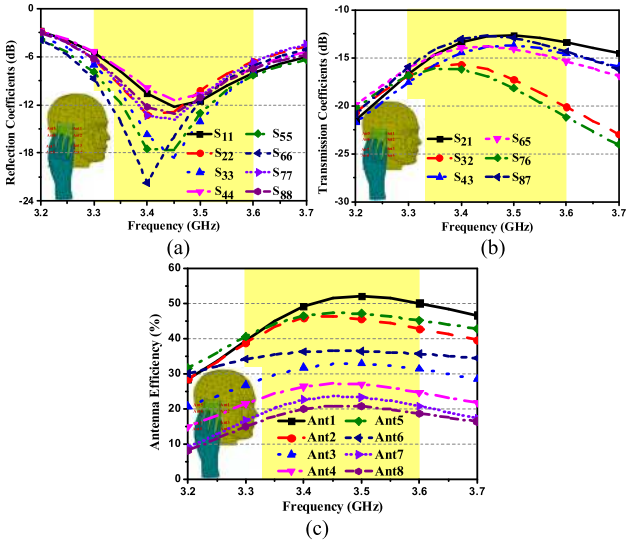

FIGURE 17. Simulated (a) reflection coefficients, (b) transmission coefficients and (c) antenna efficiencies of the MIMO array with single hand and head model.

Figs. 15, 16 and 17 show the corresponding changes of all elements' performances of the 8×8 MIMO array under different holding postures, respectively. As indicated in Figs. 15(a) and 16(a), the impedance matching of the proposed array is not influenced significantly due to the hands are not contact with the antennas directly, under the single and double hand holding mode. But the resonant points of some elements which are close to the hand model will slightly deviated away from the desired 3.45GHz, such as the S_{44}, S_{77}, and S_{88} in Fig. 15(a). So does the head model mode.

However, some of the isolations between antenna elements get worse maybe due to the hand model loading. In addition, in terms of the antenna efficiencies, the hand and head model can be equivalent to the irregular lossy medium, so a part of the radiation power of antenna is absorbed by the medium, causing the decline of the antenna efficiencies, as shown in Figs. 15(c), 16(c), and 17(c). The efficiencies of some elements which are adjacent to the medium are reduced to below 30% due to the absorption of hand and head medium. Besides, it can be obviously known from the simulated results that the array performances are closely related to the distance between antenna elements and the hand or the head model. The closer the distance is, the greater impact on the bandwidth and the efficiencies will be. Even though, the antenna elements that away from the medium still have good radiation capability and ideal antenna efficiency, such as the Ant 1, 2, 5, 6 in Fig. 15(c) and the Ant6, 7 in Fig. 16 (c). As a result, the proposed 8×8 MIMO antenna array is suitable for 5G mobile terminal applications.

IV. CONCLUSION

In this paper, a high isolation eight-element MIMO array for 5G smartphone applications has been proposed and investigated. The proposed array shows a good return loss lower than 6dB. And an acceptable radiating efficiency over 40% is obtained. The isolations, better than 15dB, are achieved by hybrid decoupling structure in the array. And a good radiation pattern and the gain characteristics of two types of elements are obtained. Meanwhile, the ECC is less than 0.15 and the calculated channel capacity of the eight-element array is about 35bps/Hz with 20dB SNR for the desired band of 3.3-3.6GHz. Meanwhile, the effect of user's hand and head has been analyzed as well. Due to good performances in bandwidth, isolation, efficiency, channel capacity and small size, the proposed eight-element MIMO array is a prospective candidate for 5G smartphone applications.

REFERENCES

[1] S. Q. Li, "5G: Intelligent mobile communication 1.0," *ZTE Technol.*, vol. 22, no. 3, pp. 47–48, Jun. 2016.

[2] H. J. Li *et al.*, "Cooperative management architecture and mechanism of 55G oriented distributed mobile cloud computing G-oriented," *ZTE Technol.*, vol. 21, no. 2, pp. 14–19, Apr. 2015.

[3] A. A. Al-Hadi, J. Ilvonen, R. Valkonen, and V. Viikari, "Eight-element antenna array for diversity and MIMO mobile terminal in LTE 3500 MHz band," *Microw. Opt. Technol. Lett.*, vol. 56, no. 6, pp. 1323–1327, Jun. 2014.

[4] K.-L. Wong, T.-W. Kang, and M.-F. Tu, "Internal mobile phone antenna array for LTE/WWAN and LTE MIMO operations," *Microw. Opt. Technol. Lett.*, vol. 53, no. 7, pp. 1569–1573, Jul. 2011.

[5] M. A. Jensen and J. W. Wallace, "A review of antennas and propagation for MIMO wireless communications," *IEEE Trans. Antennas Propag.*, vol. 52, no. 11, pp. 2810–2824, Nov. 2004.

[6] A. Ramachandran, S. V. Pushpakaran, M. Pezholil, and V. Kesavath, "A four-port MIMO antenna using concentric square-ring patches loaded with CSRR for high isolation," *IEEE Antennas Wireless Propag. Lett.*, vol. 15, pp. 1196–1199, Nov. 2016.

[7] Z. Li, Z. Du, M. Takahashi, K. Saito, and K. Ito, "Reducing mutual coupling of MIMO antennas with parasitic elements for mobile terminals," *IEEE Trans. Antennas Propag.*, vol. 60, no. 2, pp. 473–481, Feb. 2012.

[8] M.-Y. Li *et al.*, "Eight-port orthogonally dual-polarized antenna array for 5G smartphone applications," *IEEE Trans. Antennas Propag.*, vol. 64, no. 9, pp. 3820–3830, Sep. 2016.

[9] M.-Y. Li, Y.-L. Ban, Z.-Q. Xu, J. Guo, and Z.-F. Yu, "Tri-polarized 12-antenna MIMO array for future 5G smartphone applications," *IEEE Access*, vol. 6, pp. 6160–6170, Dec. 2017.

[10] K.-L. Wong and J. Y. Lu, "3.6-GHz 10-antenna array for MIMO operation in the smartphone," *Microw. Opt. Technol. Lett.*, vol. 57, no. 7, pp. 1699–1704, Jul. 2015.

[11] K. L. Wong, J.-Y. Lu, L.-Y. Chen, W.-Y. Li, and Y.-L. Ban, "8-antenna and 16-antenna arrays using the quad-antenna linear array as a building block for the 3.5-GHz LTE MIMO operation in the smartphone," *Microw. Opt. Technol. Lett.*, vol. 58, no. 1, pp. 174–181, Jan. 2016.

[12] S. Zhang, A. A. Glazunov, Z. Ying, and S. He, "Reduction of the envelope correlation coefficient with improved total efficiency for mobile LTE MIMO antenna arrays: Mutual scattering mode," *IEEE Trans. Antennas Propag.*, vol. 61, no. 6, pp. 3280–3291, Jun. 2013.

[13] L. Zhao and K.-L. Wu, "A dual-band coupled resonator decoupling network for two coupled antennas," *IEEE Trans. Antennas Propag.*, vol. 63, no. 7, pp. 2843–2850, Jul. 2015.

[14] A. Boukarkar, X. Q. Lin, Y. Jiang, L. Y. Nie, P. Mei, and Y. Q. Yu, "A miniaturized extremely close-spaced four-element dual-band MIMO antenna system with polarization and pattern diversity," *IEEE Antennas Wireless Propag. Lett.*, vol. 17, no. 1, pp. 134–137, Nov. 2017.

[15] Y.-L. Ban, C. Li, C.-Y.-D. Sim, G. Wu, and K.-L. Wong, "4G/5G multiple antennas for future multi-mode smartphone applications," *IEEE Access*, vol. 4, pp. 2981–2988, Jun. 2016.

[16] K.-L. Wong, C.-Y. Tsai, and J.-Y. Lu, "Two asymmetrically mirrored gap-coupled loop antennas as a compact building block for eight-antenna MIMO array in the future smartphone," *IEEE Trans. Antennas Propag.*, vol. 65, no. 4, pp. 1765–1778, Apr. 2017.

[17] Y. Li, C.-Y.-D. Sim, Y. Luo, and G. Yang, "12-Port 5G massive MIMO antenna array in Sub-6GHz mobile handset for LTE bands 42/43/46 applications," *IEEE Access*, vol. 6, pp. 344–354, Oct. 2017.

[18] J. Prakash, R. Vijay, and S. Natarajamani, "MIMO antenna for mobile terminals with enhanced isolation in LTE band," in *Proc. Int. Conf. Adv. Comput., Commun. Inform.*, Udupi, India, Sep. 2017, pp. 2231–2234.

[19] Y. Wang and Z. Du, "A wideband printed dual-antenna with three neutralization lines for mobile terminals," *IEEE Trans. Antennas Propag.*, vol. 62, no. 3, pp. 1495–1500, Mar. 2014.

[20] X. Ling and R. Li , "A novel dual-band MIMO antenna array with low mutual coupling for portable wireless devices," *IEEE Antennas Wireless Propag. Lett.*, vol. 10, pp. 1039–1042, Sep. 2011.

[21] H. Huang, X. Li, and Y. Liu, "5G MIMO antenna based on vector synthetic mechanism," *IEEE Antennas Wireless Propag. Lett.*, vol. 17, no. 6, pp. 1052–1055, Jun. 2018.

[22] Y. Li, C. Wang, H. Yuan, N. Liu, H. Zhao, and X. Li, "A 5G MIMO antenna manufactured by 3-D printing method," *IEEE Antennas Wireless Propag. Lett.*, vol. 16, pp. 657–660, Jul. 2016.

[23] X. Zhao, S. P. Yeo, and L. C. Ong, "Decoupling of inverted-F antennas with high-order modes of ground plane for 5G mobile MIMO platform," *IEEE Trans. Antennas Propag.*, vol. 66, no. 9, pp. 4485–4495, Jun. 2018.

[24] M. S. Sharawi, M. Ikram, and A. Shamim, "A two concentric slot loop based connected array MIMO antenna system for 4G/5G terminals," *IEEE Trans. Antennas Propag.*, vol. 65, no. 12, pp. 6679–6686, Dec. 2017.

[25] S. Nandi and A. Mohan, "A compact dual-band MIMO slot antenna for WLAN applications," *IEEE Antennas Wireless Propag. Lett.*, vol. 16, pp. 2457–2460, Jun. 2017.

[26] J. Y. Deng, J. Li, L. Zhao, and L. Guo, "A dual-band inverted-F MIMO antenna with enhanced isolation for WLAN applications," *IEEE Antennas Wireless Propag. Lett.*, vol. 16, pp. 2270–2273, Jun. 2017.

[27] J. Dong, X. Yu, and L. Deng, "A decoupled multiband dual-antenna system for WWAN/LTE smartphone applications," *IEEE Antennas Wireless Propag. Lett.*, vol. 16, pp. 1528–1532, Jan. 2017.

[28] C. F. Ding, X. Y. Zhang, C.-D. Xue, and C.-Y.-D. Sim, "Novel pattern-diversity-based decoupling method and its application to multielement MIMO antenna," *IEEE Trans. Antennas Propag.*, vol. 66, no. 10, pp. 4976–4985, Oct. 2018.

[29] L. B. Sun, H. Feng, Y. Li, and Z. Zhang, "Compact 5G MIMO mobile phone antennas with tightly arranged orthogonal-mode pairs," *IEEE Trans. Antennas Propag.*, vol. 66, no. 11, pp. 6364–6369, Nov. 2018.

[30] J.-H. Xun, L.-F. Shi, W.-R. Liu, G.-X. Liu, and S. Chen, "Compact dual-band decoupling structure for improving mutual coupling of closely placed PIFAs," *IEEE Antennas Wireless Propag. Lett.*, vol. 16, pp. 1985–1989, Apr. 2017.
[31] C.-D. Xue, X. Y. Zhang, Y. F. Cao, Z. Hou, and C. F. Ding, "MIMO antenna using hybrid electric and magnetic coupling for isolation enhancement," *IEEE Trans. Antennas Propag.*, vol. 65, no. 10, pp. 5162–5170, Oct. 2017.
[32] K.-L. Wong, Y.-C. Chen, and W.-Y. Li, "Four LTE low-band smartphone antennas and their MIMO performance with user's hand presence," *Microw. Opt. Technol. Lett.*, vol. 58, pp. 2046–2052, Sep. 2016.

WEN JIANG was born in Shandong, China, in 1985. He received the B.S. and Ph.D. degrees from Xidian University, Xi'an, China, in 2008 and 2012, respectively, where he is currently the Vice Director of the National Key Laboratory of Science and Technology on Antennas and Microwaves and also an Associate Professor. His current research interests include electromagnetic scattering theory and technology, antenna theory and engineering, and electromagnetic measurement theory and technology.

BO LIU was born in Shaanxi, China, in 1994. He received the B.S. degree in electromagnetic field and microwave technology from Xidian University, Xi'an, China, in 2017, where he is currently pursuing the M.S. degree. His main research interests are MIMO smartphone antennas and millimeter wave terminal antennas for 5G mobile communications, and multiband smartphone antennas.

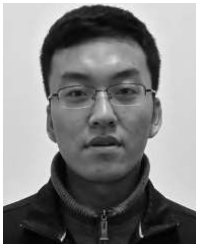

YANGQIANG CUI was born in Shanxi, China, in 1995. He received the B.S. degree in electronic information engineering from Xidian University, Xi'an, China, in 2017, where he is currently pursuing the M.S. degree with the School of Electronics and Communication Engineering. His current research interests include MIMO antenna theory and design.

WEI HU received the B.S. degree in electronic information engineering and the Ph.D. degree in electromagnetic wave and microwave technology from Xidian University, Xi'an, China, in 2008 and 2013, respectively.

He is currently an Associate Professor with the National Laboratory of Science and Technology on Antennas and Microwaves, Xidian University. His research interests include multiband and wideband antennas, circularly polarized and dual-polarized antennas, and MIMO technologies.